



Chloride induced reinforcement corrosion: Electrochemical monitoring of initiation stage and chloride threshold values

Ueli M. Angst^{a,*}, Bernhard Elsener^{b,c}, Claus K. Larsen^{a,d}, Øystein Vennesland^a

^a NTNU Norwegian University of Science and Technology, Department of Structural Engineering, Richard Birkelandsvei 1A, N-7491 Trondheim, Norway

^b ETH Zurich, Institute for Building Materials (IfB), ETH Hönggerberg, CH-8093 Zurich, Switzerland

^c University of Cagliari, Department of Inorganic and Analytical Chemistry, I-09142 Monserrato, Cagliari, Italy

^d Norwegian Public Roads Administration, N-0033 Oslo, Norway

ARTICLE INFO

Article history:

Received 5 November 2010

Accepted 13 January 2011

Available online 21 January 2011

Keywords:

A. Steel reinforced concrete

B. Polarisation

C. Pitting corrosion

C. Repassivation

ABSTRACT

Reinforcement steel embedded in six different concrete mixes was exposed to chloride by wetting/drying cycles. Various parameters were continuously monitored during more than 1 year. Cement replacement with fly ash had beneficial long-term effects regarding chloride penetration resistance. Concerning corrosion performance, by far the most dominant influencing parameter was the steel/concrete interface since corrosion initiated on the lower side of the rebar (with respect to casting direction) regardless of binder type and w/b ratio. In many cases, after the first signs of depassivation, a marked increase in chloride content was required to prevent repassivation and to enable stable pit growth.

© 2011 Elsevier Ltd. All rights reserved.

1. Introduction

Penetration of chloride from seawater or de-icing salts into concrete and the associated risk for reinforcement corrosion is in many countries regarded as the most important degradation mechanism for reinforced concrete infrastructure. From an engineering viewpoint, the service life is usually divided into an initiation phase and a propagation phase [1]. The initiation phase describes chloride ingress and is terminated by depassivation of the reinforcement, which then marks the beginning of the propagation stage.

Chloride induced corrosion of reinforcement in concrete has over several decades been extensively studied under field and laboratory conditions, particularly regarding the so-called critical chloride content or chloride threshold value (both terms have in this paper the same meaning) [2,3]. This value corresponds to the chloride content measured at the rebar depth at the transition from initiation stage to propagation stage, i.e. the chloride content associated with depassivation of the reinforcement. It is affected by numerous interrelated parameters, among them properties of the steel/concrete interface, pore solution chemistry and the steel potential. These variables are in turn affected by concrete characteristics such as the water/binder ratio (w/b) or binder type. The performance of a structure exposed to chlorides is, however, not

only determined by the critical chloride content, but depends also on the thickness and quality of the concrete cover. The denser the concrete, the more time will pass until the critical chloride content is reached at the steel surface. Also this can be controlled by mix design, e.g. by varying w/b ratio and binder type. Finally, the corrosion rate during propagation is affected by concrete parameters as well. In some cases, e.g. when using pozzolanic materials such as fly ash, the microstructure might be denser and thus more penetration-resistant while at the same time the pH in the pore solution is decreased, which negatively affects the chloride threshold value [4]. Holistic assessment of concrete mixes regarding durability should thus involve characterisation of the penetration resistance against chlorides, measurement of the critical chloride content and the parameters that govern the degradation rate during the propagation stage.

In this work, a common setup based on chloride ingress by wetting/drying cycles was used to study the initiation stage of chloride induced reinforcement corrosion in several concrete mixes. Portland cement (PC) and sulphate resistant (SR) cement as well as these binders in combination with fly ash (FA) were investigated. The chloride concentration in the pore solution, the electrical concrete resistivity as well as several electrochemical parameters of the embedded reinforcement steel were non-destructively and continuously monitored. This allows characterising the performance of the studied concrete mixes regarding their resistance towards chloride induced reinforcement corrosion.

* Corresponding author. Tel.: +47 735 94 538; fax: +47 735 94 701.

E-mail address: ueli.angst@ntnu.no (U.M. Angst).

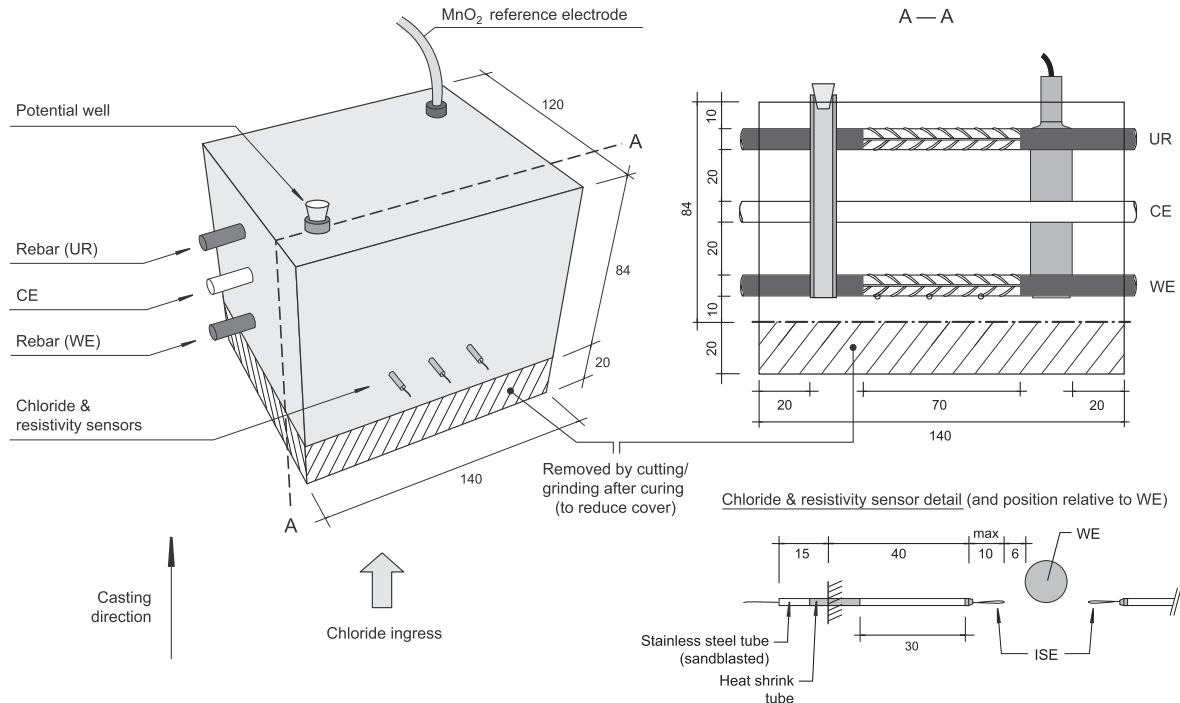


Fig. 1. Specimen geometry and embedded rebars and sensors (dimensions in mm). Chloride ingress from bottom side (WE) after curing.

Table 1
Nominal mix proportions (calculated by assuming 1.5 vol.% air).

Mix label	PC-04	PC-06	PC-05	SR-05	PCFA-05	SRFA-05
Binder	100% PC	100% PC	100% PC	100% SR	100% PCFA	80% SR + 20% FA
w/b	0.4	0.6	0.5	0.5	0.5	0.5
Water (kg/m ³)	196	230	215	216	211	211
Binder (kg/m ³)	490	383	430	432	422	337 + 84
Aggregates 0–8 (kg/m ³)	1707	1707	1707	1707	1707	1707
Superplasticizer (% by cement weight)	1.3 ^a	0.25 ^a	0.8 ^a	0.9 ^a	1.0 ^b	0.7 ^a

^a Glenium 151 (BASF Norway).

^b Mighty 150 (Kao Industrial Thailand).

2. Experimental

2.1. Materials and specimens

Concrete specimens with two embedded rebars ($\varnothing 8$ mm) of ordinary reinforcing steel (B500C, ribbed) and one stainless steel bar (type 1.4301/304L) were cast with dimensions given in Fig. 1. The steel was used in as-received condition. To avoid boundary effects, the ends of the rebars were shielded by a similar system as the one described by Lambert et al. [5,6]: A coating of abrasion-resistant cement paste (made by mixing Portland cement and a styrene-butadiene co-polymer emulsion in a ratio of 3:2 by volume) was applied to the end parts of the rebars and, after 1 d of hardening, masked with a heat-shrink tube in order to prevent access of chloride ions. The exposed length between the end shielding was 7 cm and the rebar area thus ca. 17.6 cm². Visual inspection after terminating the experiments confirmed that the two-layer system was suitable to avoid crevice corrosion under the heat-shrink tube. Since the rebar on the sample side later exposed to chloride ingress (lower side in Fig. 1) was the working electrode of primary interest it was denoted WE; the upper rebar was referred to as UR and the stainless steel bar that was used as counter electrode for polarisation experiments was denoted CE (Fig. 1). Note that casting was performed with the specimen upside down with respect to Fig. 1.

For monitoring purposes, each sample was instrumented with a manganese dioxide reference electrode (Force Technology, ERE 20) as well as six combined chloride/resistivity sensors [7] (three on

Table 2
Properties of used cements and pozzolanas (according to supplier).

	Portland cement (PC)	Sulphate resistant cement (SR)	Fly ash cement (PCFA)	Fly ash (FA)
EN 197-1	CEM I 52.5 N	CEM I 42.5 R	CEM II/A-V 42.5 N	–
Blaine fineness (m ² /kg)	360	440	370	390
C ₃ A	6%	0.5%	–	–
Na ₂ O equivalent	0.55%	0.53%	0.48% ^a	2.59%
Chloride content	<0.08%	<0.08%	<0.09%	–
Remarks	–	–	79.2% PC + 20.8%FA	Class F SiO ₂ = 54.4% Al ₂ O ₃ = 22.0% Fe ₂ O ₃ = 5.8% CaO = 4.8% K ₂ O = 2.2% Na ₂ O = 1.2%

^a Alkali content in clinker.

Table 3
Properties of fresh and hardened concretes.

		PC-04	PC-06	PC-05	SR-05	PCFA-05	SRFA-05
Slump (± 20 mm)	EN 12350-2	220	180	190	200	230	190
Density (g/l)	EN 12350-6	2382	2287	2333	2341	2330	2298
Air content (vol.%)	EN 12350-7	4.0	4.5	3.9	4.1	5.7	6.1
Compressive strength at 28 d (MPa) ^a		80.7	49.4	72.5	73.0	53.7	58.2

^a Self-desiccated state.

each side). These sensors consist of chloride ion selective electrodes (ISE), mounted in stainless steel tubes that allow measurement of the electrical resistance between two tubes and can thus be used to monitor the concrete resistivity (Fig. 1). The exposed length of each steel tube is 30 mm (on the back side shielded with a heat-shrink tube), with an outer diameter of 2.5 mm; the distance between the tubes is 20 mm. The ISEs allow non-destructive measurement of the chloride ion activity in the pore solution. Further details on the functionality and application of ISEs to concrete can be found in earlier publications by the present authors [7,8].

Six different concrete mixes were studied with the proportions given in Table 1. Properties of the used binders are given in Table 2. Norwegian aggregates (Årdal 0–8 mm, Gneiss) were used, that have a filler content of 7% by weight (particles < 0.125 mm). Properties of the fresh concretes are reported in Table 3. In the presence of fly ash, the air content increased during mixing; in the case of the commercial fly ash cement (PCFA), another type of superplasticizer had to be used in order to minimise the air content. The relatively high slumps of the fresh mixes allowed careful casting and compaction in order not to harm the sensors installed in the moulds. The concrete was filled into the moulds in layers and each compacted on a vibration table during ca. 15 s. A set of three additional cubes (10^3 cm^3) was cast from each mix (same batch) for testing the compressive strength at the age of 28 d (Table 3).

For each of the six concrete mixes, four parallel samples (Fig. 1) were cast in custom-made plywood moulds, demoulded after 1 d, and sealed in plastic for curing at 20 °C (self-desiccation). Before casting, all the steel bars, sensors and reference electrodes as well as a round Teflon bar were fixed in the mould. At the time of demoulding, the Teflon bar was drawn out of the concrete and a plastic hose immediately glued into the remaining hole in order to seal the inner, lateral surfaces of the hole. The upper opening was closed with a removable rubber plug in order to minimise drying and carbonation of the concrete inside the hole. This so-called *potential well* was later used to insert an external reference electrode and place its tip on the bottom concrete surface of the hole for additional potential measurements.

At the age of 28 d, the cover of WE was reduced from initially 30 to 10 mm by diamond cutting and grinding (Fig. 1). This ensured a realistic cover depth during casting, compaction and curing, but accelerated chloride ingress by reducing the cover and removing the outer cement skin formed at the mould. The chloride/resistivity sensors, the tip of the embedded MnO_2 reference electrode as well as the bottom of the *potential well* were all at the same depth, namely 10 mm, which is the concrete cover of WE after cutting. No cracks were visually detected after cutting. The lateral surfaces of the samples were painted with an epoxy-resin to ensure one-dimensional transport processes (only top and bottom faces exposed to air or solution).

The six mixes are denoted according to Table 1 and the four parallel specimens of each mix are referred to as, for instance, PC-04-1, i.e. sample #1 of mix PC-04.

2.2. Chloride exposure and measurements

Right after demoulding the samples, all sensor and rebar potentials were measured manually. At the age of 42 d, the samples were

exposed to weekly wetting/drying cycles, in which the sample surface on the side of WE was placed in a chloride solution (prepared by adding sodium chloride to tap water) during 2 d and exposed to air (laboratory environment) for 5 d (Fig. 1). The chloride concentration in the exposure solution was varied over time as will be indicated together with the results.

The set of totally 24 specimens was connected to a data logging system that allowed continuous and simultaneous measurement of the following parameters; per specimen:

- 8 potentials: WE, UR, and 6 ISEs.
- 2 electrical resistances (between two adjacent, parallel stainless steel tubes on each side).
- Linear polarisation resistance (R_p) of WE.

The interval between automatic recordings of these parameters was initially 6 h, and later increased to 12 h. Potentials were measured against the embedded MnO_2 reference electrode. Occasionally, manual measurements were carried out vs. an external saturated calomel electrode (SCE) that was temporarily inserted in the *potential well*. This allows expressing all potentials vs. SCE rather than the embedded MnO_2 reference electrodes, which have different potentials from electrode to electrode. To establish contact between concrete and SCE, a thin piece of cloth was placed on the bottom of the *potential well* and wetted with a droplet of 0.35 M KOH. Regarding ISE potentials, corrections for liquid junction potentials at the interface SCE/0.35 M KOH/pore solution were made and the results converted into chloride ion activity as described elsewhere [8]. For the liquid junction potential, a value of 5.5 mV was assumed for Portland and sulphate resistance cement mixes; in the case of fly ash containing mixes, 3.5 mV was used owing to the lower pH in the pore solution.

All potentials apart from WE were measured with analogue voltage logging modules from National Instruments (input impedance $10^{10} \Omega$). Electrical resistance measurements between sensor steel tubes as well as potential and linear polarisation resistance measurements of WE were automatically performed by equipment provided by the company Protector AS. The electrical resistances between steel tubes were measured with alternating current (sinusoidal signal) at a frequency of 1 kHz. The polarisation resistance (R_p) was determined by cyclic polarisation (step size 2 mV, scan rate 0.1 mV/s) of WE 10 mV into anodic and cathodic direction (starting at the corrosion potential). Due to instrumental limitations of the datalogger, correct polarisation resistances could only be measured below ca. 30 k Ω (with the present steel area this corresponds to ca. 500 k $\Omega \text{ cm}^2$). The upper instrumental limit of measurable values is 100 k Ω (ca. 2 M $\Omega \text{ cm}^2$), however, as the resolution in this range is low, R_p values measured between ca. 30 and 100 k Ω scatter considerably. Thus, correct R_p values cannot be measured in the present setup as long as the rebar is passive. Nevertheless, depassivation detection by LPR measurements was possible, however with a certain delay, since the actively corroding area has to reach a state at which it is able to depress the overall R_p below 30 k Ω . Occasionally, electrochemical impedance spectroscopy (EIS) and additional linear polarisation measurements were carried out with a Princeton Applied Research Parstat 2273 instrument that has a much higher

resolution and allows correct determination of R_p also in the passive state.

Corrections for IR drop were made numerically after the measurements: EIS was carried out on selected samples at various ages

(AC amplitude 10 mV, frequency range 2 MHz–100 μ Hz); from the diameter of the first semi-circle in the complex plane plot, the ohmic resistance in the AC current field of the relevant electrode configuration, R_u , could be estimated as described in the literature, e.g.

Table 4
Potentials of rebar (WE) after casting and before chloride exposure (average and max/min per mix).

E_{corr} (mV vs. SCE)	PC-04	PC-06	PC-05	SR-05	PCFA-05	SRFA-05
At $t = 1$ d (demoulding)	-227 (± 18)	-279 (± 20)	-277 (+44/-96)	-266 (± 16)	-235 (± 13)	-294 (+30/-59)
At $t = 42$ d (before first wetting cycle)	-86 (± 23)	-145 (± 30)	-124 (± 33)	-138 (± 24)	-72 (± 20)	-151 (± 10)

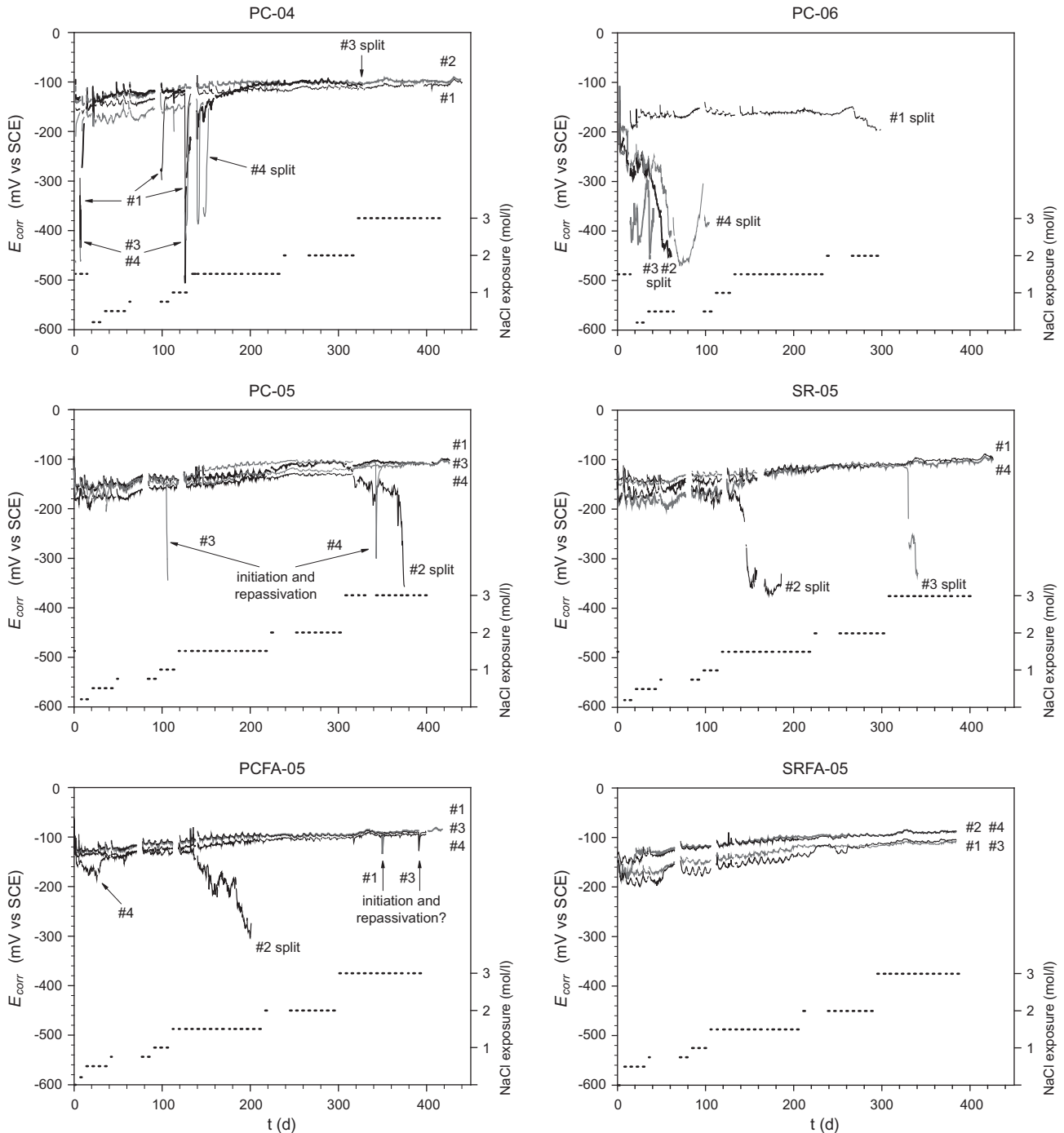


Fig. 2. E_{corr} vs. time. The four lines per plot represent the parallel samples per mix. The dashed line indicates the wetting/drying cycles (dashes = wetting with the exposure concentration given on the right ordinate; space between the dashes = drying).

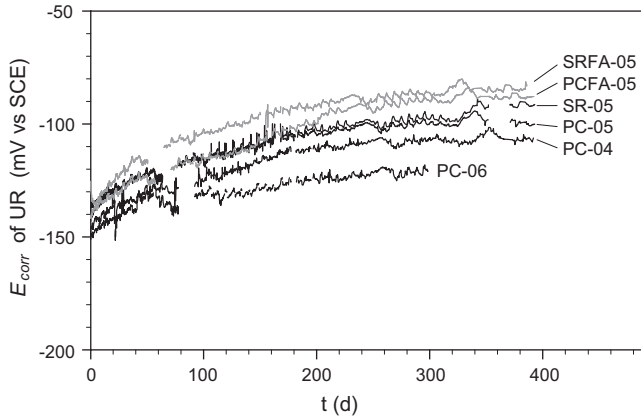


Fig. 3. Potential of upper rebar (UR) vs. time; average per mix (the standard deviation of the four values was in the range 5–15 mV).

Ref. [9]. It was found that the ratio R_u/R_{tubes} , where R_{tubes} is the electrical resistance between two adjacent, parallel sensor tubes, was ca. 0.18 ± 0.02 at most ages and independent of mix. This figure

was thus used to estimate R_u for individual mixes and as a function of time, based on continuous resistance measurements. The diameter of the second semi-circle of electrochemical impedance spectra was taken as the charge-transfer resistance (R_{ct}) which can be equated to R_p [10]. To obtain the diameter, a circle was fitted to the data.

2.3. Sampling procedure and visual examination

Once corrosion had reached a stable stage, the specimens were treated in the following way: From 14 selected samples, two concrete prisms (approximately $4 \text{ cm} \times 4 \text{ cm} \times 8.4 \text{ cm}$) were cut and the bulk resistivity measured in two directions, viz. along and perpendicular to the chloride/moisture profile, with steel plates on the parallel surfaces (contact with tap water, AC measurement with a commercial LCR meter, $f = 1 \text{ kHz}$). No significant differences were observed between the two directions. Based on these measurements, the cell constant for conversion of electrical resistance between two adjacent, parallel stainless steel tubes into concrete resistivity, ρ , was estimated at $\eta = R_{tubes}/\rho = 36 \text{ m}^{-1}$ ($\pm 20\%$). A numerical simulation with the conductive media application mode

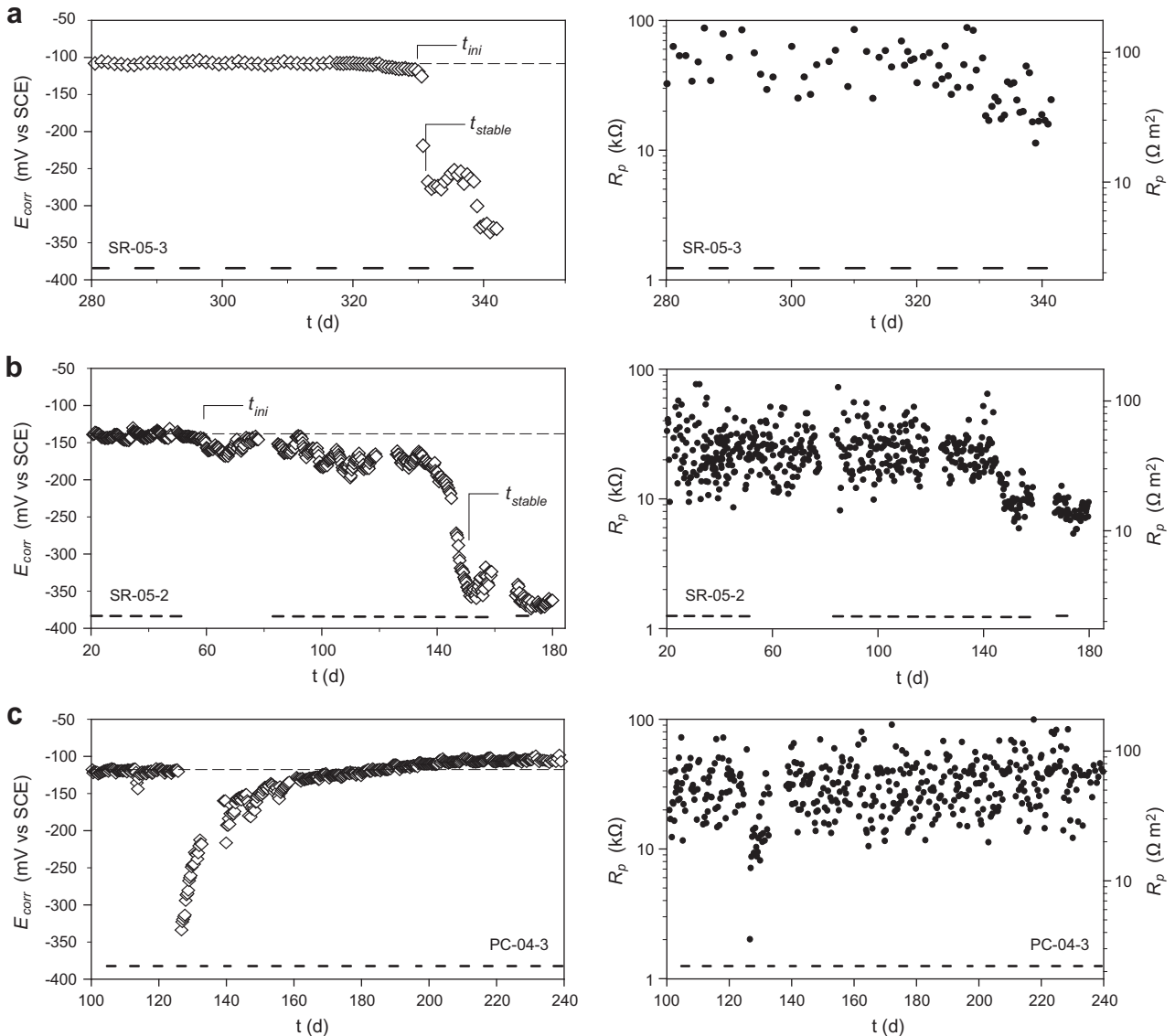


Fig. 4. Close-ups of three characteristic curves of E_{corr} and R_p vs. time indicating sudden depassivation (a), reluctant depassivation (b), and depassivation/repassivation (c). The dashed line shows the level of the stable potential in the passive state; the black dashes along the time axis represent wetting cycles.

Table 5
Time to corrosion and visual examination of rebar (WE).

Mix	Specimen	t_{mi} (d) first sign of initiation	t_{stable} (d) time to stable pitting	t_{split} (d) time of splitting	Visual inspection of steel surface (p = depth where corrosion started on the rebar)
PC-04	#1	– ^a	>447	447	No signs of corrosion
	#2	>447	>447	447	–
	#3	– ^a	>329	329	Tiny pit on upper side (p = 16 mm)
	#4	2	125 ^b	154	Small pit on upper side (p = 18 mm)
PC-06	#1	>300	>300	300	No signs of corrosion
	#2	10	41	61	Large pit on upper side (p = 18 mm)
	#3	11	13	41	Large pit(s) on upper side (p = 18 mm)
	#4	9	49	104	Pits on upper side, two sites (p = 17 mm)
PC-05	#1	>438	>438	438	–
	#2	320	372	377	Large pit on upper side (p = 16 mm), tiny pits on lower side (p = 12–14 mm)
	#3	105 ^c	>438	438	–
	#4	343 ^c	>438	438	–
SR-05	#1	>439	>439	439	–
	#2	60	147	187	Large pits on upper side (p = 18 mm)
	#3	330	331	345	Small pit on upper side (p = 17 mm)
	#4	>439	>439	439	–
PCFA-05	#1	350 ^c	>420	420	–
	#2	140	185	202	Large pit(s) on upper side (p = 18 mm)
	#3	391 ^c	>420	420	–
	#4	9 ^c	>420	420	–
SRFA-05	#1	>388	>388	388	–
	#2	>388	>388	388	–
	#3	>388	>388	388	No signs of corrosion
	#4	>388	>388	388	–

^a Initiated and repassivated several times during exposure.

^b Stable pitting only during wetting cycles, immediately stopped corroding during drying periods.

^c Followed by repassivation.

of the software COMSOL [11] yielded a theoretical cell constant $\eta = 32 \text{ m}^{-1}$. For the conversion $\eta = 34 \text{ m}^{-1}$ was used. Please note that this conversion of resistance into resistivity is only valid for drying cycles, since the cell constant is affected when the specimen is immersed in solution.

The remaining part of the sample was then vertically split along the embedded rebars for visual examination of steel and concrete surfaces, particularly the steel/concrete interface. In some samples, ca. 2 mm thin plates were cut from the immediate vicinity of the rebar (by dry-cutting) and powdered for chloride analysis. Additional samples cut from the cover zone allowed determining the chloride profile. Alternatively, when concrete prisms were sawn for resistivity measurements, chloride profiles were determined by grinding 2 mm thick layers from these prisms and collecting the powder. In each sample, two chloride profiles were measured. The total chloride content was determined as the acid-soluble chloride content (5 g concrete powder, 6.5% nitric acid, 30 s stirring at 80 °C, dissolution time 1–3 h at ambient temperature, chloride analysis by a spectrophotometric method).

3. Results

3.1. Electrochemical monitoring

Table 4 shows the potentials of WE 1 d after casting and at age 42 d right before starting the first wetting cycle. In all cases, potentials reached -150 to -70 mV vs. SCE and passivity had established during this period. Figs. 2 and 3 show the steel potentials during the subsequent wetting/drying exposure of the rebar on the exposed side (WE) and the upper rebar (UR), respectively. In the passive state, the potential was generally stable with a tendency to increase over time for all mixes. This is most pronounced in fly ash containing mixes and least pronounced in mix PC-06. The

increase occurred independent of exposure to wetting/drying cycles (WE) or constant exposure to dry laboratory environment (UR).

Corrosion onset was apparent from a fall in potential. In this work, three different cases have been observed. Fig. 4 depicts examples of these with the relevant fraction of the time-scale for reasons of clarity:

- Sudden drop in potential:** In two samples (PC-06-3, SR-05-3), E_{corr} dropped by ca. 200 mV within 1 or 2 d and from then on stayed on a clearly more negative level than in the passive state.
- Slow potential decrease:** E_{corr} diminishes moderately, viz. by a few tens of millivolts with respect to the passive level, and only after 3–9 more wetting/drying cycles, a drop to clearly

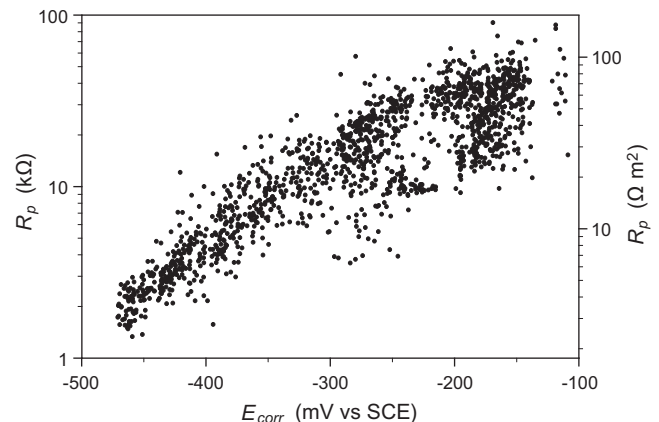


Fig. 5. Relationship between R_p and E_{corr} during transition from passive to active state. Data of all samples after depassivation.

lower potentials occurs. In this study, this depassivation behaviour was observed in samples PC-06-2, PC-06-4, PC-05-2, SR-05-2, and PCFA-05-2.

(c) *Depassivation/repassivation*: Fig. 4c shows an example of depassivation followed by repassivation. In some samples, the rebar depassivated once more several wetting/drying cycles later, i.e. at a higher chloride concentration, or sometimes remained passive for several months or even the rest of the exposure procedure. Such depassivation/repassivation events were observed in samples PC-04-1, PC-04-3, PC-04-4, PC-05-3, PC-05-4, PCFA-05-1, PCFA-05-3, and PCFA-05-4.

For each sample, Table 5 gives the time, t_{ini} , at which the first signs of corrosion initiation were observed by electrochemical measurements, viz. a tendency towards falling potential. The time

at which the potential dropped to clearly more negative potentials (by 200–300 mV) was here termed t_{stable} , assuming that by then stable pitting is likely to continue without further wetting cycles. The samples were then observed during some further weeks and split for visual inspection and analysis of acid-soluble chloride at t_{split} . The respective values are also given in Table 5. While in case (a) with a sudden potential drop, the difference between t_{ini} and t_{stable} is small (Fig. 4a), in case (b) with samples exhibiting a slow potential decrease, considerable amount of time might pass from t_{ini} to t_{stable} . In the example shown in Fig. 4b, ca. 9 wetting/drying cycles were required to depassivate WE; without further chloride ingress, the sample had a tendency to repassivate (as apparent from the long drying cycle up to ca. 80 d).

Depassivation could also be detected by the automatic LPR measurements since R_p essentially followed the potential decrease.

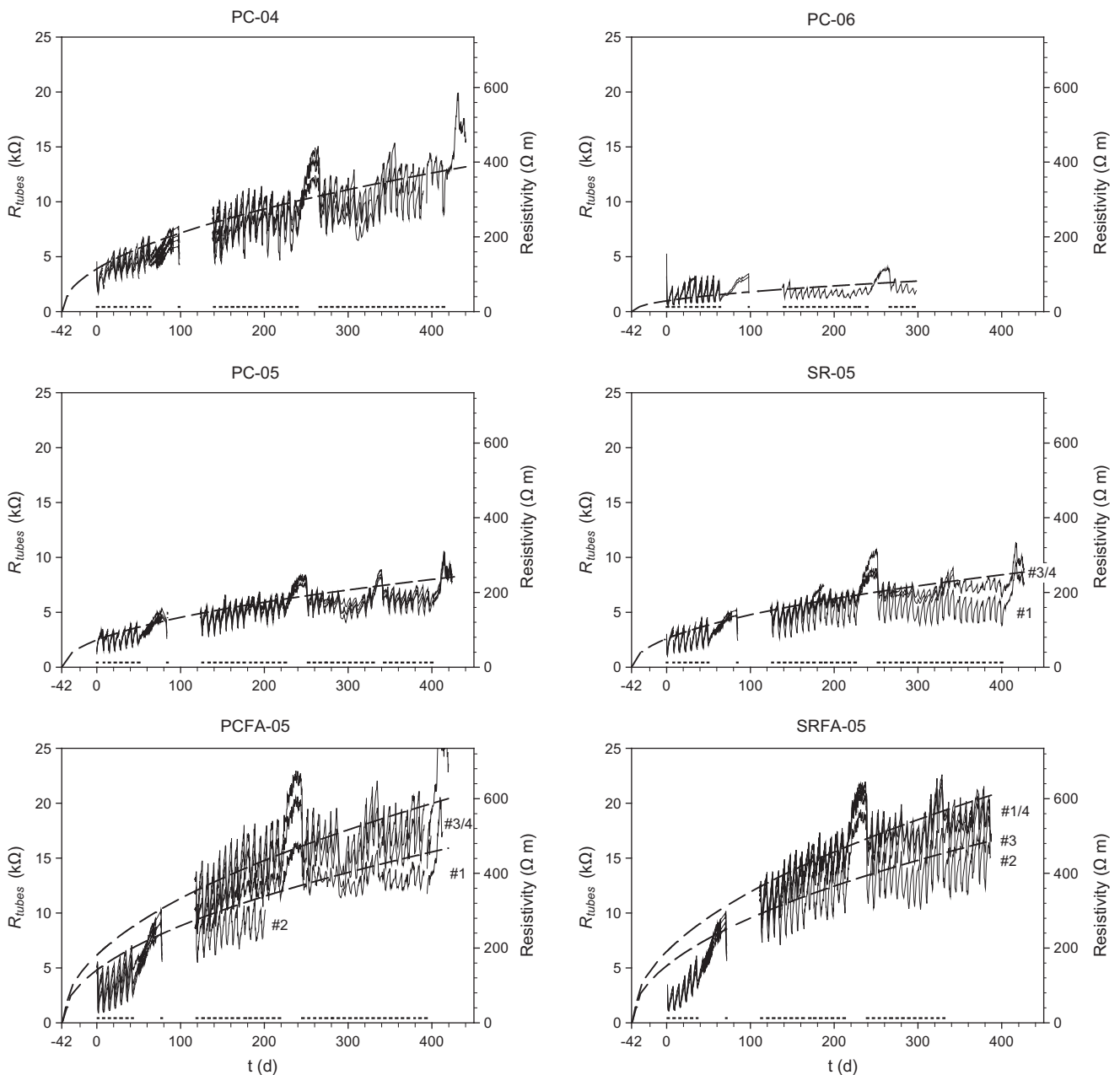


Fig. 6. Electrical resistance and resistivity of the different mixes vs. time. One curve per concrete specimen (average of two measured values per specimen). The dashes on the lower border of the graphs indicate wetting, the space between the dashes drying. The long dashed curves are fits with \sqrt{t} -law.

This can be seen from the plots on the right hand side in Fig. 4. However, owing to the inaccuracy of the measurements in the passive state (compare Section 2.2) and the associated scatter of R_p (Fig. 4), identification of t_{ini} and t_{stable} is more difficult. Occasional measurements with the potentiostat, both EIS and LPR, confirmed that in the passive state R_{ct} and R_p , respectively, were clearly higher than after the observed fall in potential. Fig. 5 shows that more negative potentials are associated with lower polarisation resistances. Thus, in this work, no other effects than depassivation of WE were responsible for decreasing E_{corr} .

Please note that in Figs. 2 and 3 (and also subsequent graphs of monitoring results) as well as in Table 5, $t = 0$ corresponds to the beginning of exposure to chloride and not to sample age. At $t = 0$, the samples had already been cured for 42 d. Regarding exposure cycles, it might be noted that they were in general comparable (Fig. 2); the only difference was that the chloride concentration during the first wetting cycles was higher in PC-06 and PC-04 than in the other series. It might in this context be worth mentioning, that the specimens appear to be particularly vulnerable at young ages (although young here means >42 d): In both series, 3 out of 4 samples depassivated during the first wetting cycles (E_{corr} 200–300 mV lower than in passive state), where comparatively high exposure concentrations were used. All of the PC-04 samples, however, recovered and two of them even remained passive for the rest of the experiments.

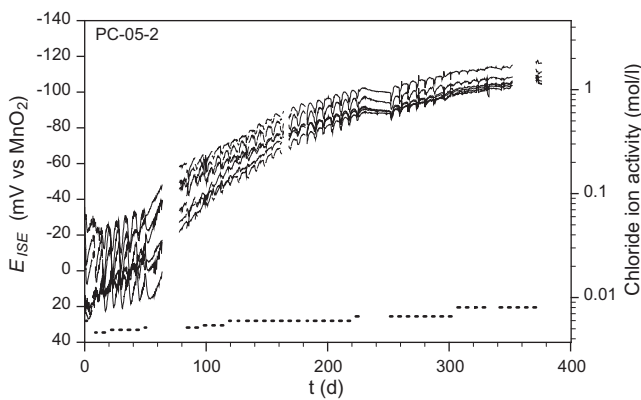


Fig. 7. Example of non-destructive monitoring of the chloride ion activity in a sample until splitting: Potentials of six ISEs vs. time as well as conversion into chloride ion activity. The dashed line qualitatively indicates the wetting/drying cycles (compare Fig. 2).

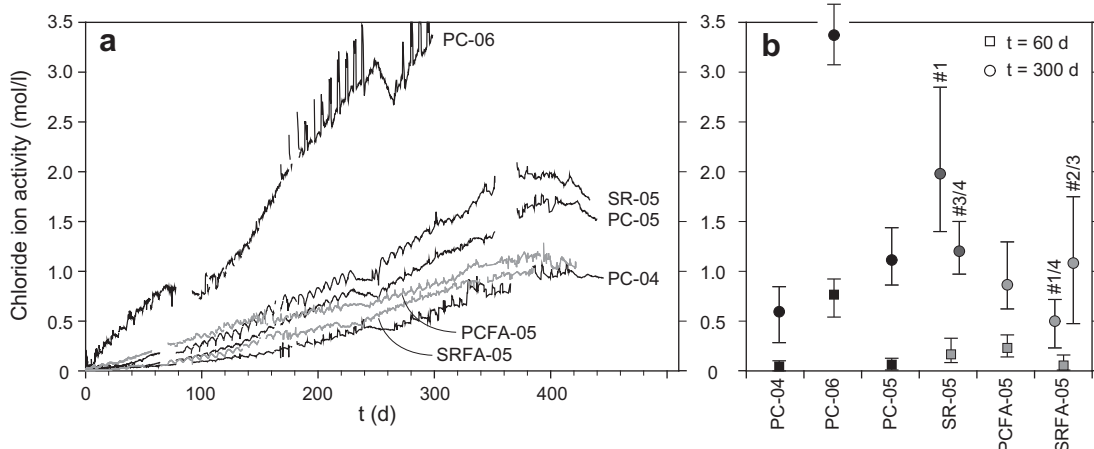


Fig. 8. Chloride ion activity in pore solution; (a) average of all ISEs per mix vs. time; (b) at $t = 60$ and 300 d, respectively, showing mean values (squares, circles) and 10% and 90% percentiles (whiskers).

3.2. Monitoring concrete resistivity

Fig. 6 shows the electrical concrete resistance measured between the steel tubes as well as the concrete resistivity (obtained by using the cell constant $\eta = 34 \text{ m}^{-1}$). The highest concrete resistivities were reached by fly ash containing mixes. In the absence of fly ash, the resistivity increased with decreasing w/c ratio, with a remarkable increase from PC-06 to PC-05. In all mixes, including PC-06, the measured resistance increased continuously with time during at least 250 d (i.e. to an age of >~300 d when including the curing period before chloride exposure). This increase with time can reasonably be described by a \sqrt{t} -law, as indicated by the fitted curves (long dashes) in Fig. 6. The periodic fluctuations in Fig. 6 reflect the wetting/drying cycles.

For some reason, the resistivities obtained from the four individual samples scatter much less in series PC-04, PC-05, and PC-06 than in SR-05, PCFA-05, and SRFA-05. For instance, in series PCFA-05 and SRFA-05, the resistance in one or two samples is ca. 20–30% lower than in the parallel samples. While for PCFA-05, this individual behaviour could be explained by the differences in measured cell constants η (Section 2.3), this was not possible for the other mixes.

3.3. Monitoring the free chloride content

Fig. 7 shows six embedded ISEs in a concrete sample vs. time as well as conversion into chloride ion activity in the pore solution. Specimen PC-05-2 is shown as an example, but the other samples gave essentially the same results. The effect of wetting/drying cycles is clearly visible. Also the scatter between the six sensors embedded in this sample is apparent: Right before splitting, the values range from 1.1 to 1.8 mol/l. Fig. 8 depicts the mean values of ISEs within each mix; in the beginning, $4 \times 6 = 24$ values were available per mix, but at later stages, whenever a specimen was removed for visual examination and sampling, the mean value was calculated from the remaining ISEs. Fig. 8b shows the free chlorides in the pore solution at two selected points in time. At an early stage, $t = 60$ d, only in series PC-06, a relatively high chloride concentration was present at 10 mm depth. Further wetting/drying cycles were able to raise the chloride ion activity in the pore solution considerably in all mixes. While the overall scatter in Portland cement samples approximates the scatter within the individual concrete specimens, particularly in series SR-05 and SRFA-05, the rate of chloride uptake differed from sample to sample. It is noticeable that those samples with a faster increase in chloride concentration

also had a lower concrete resistivity than the other parallel samples (compare Fig. 6).

3.4. Visual examination

As apparent from Table 5, during more than 1 year of chloride exposure, stable corrosion initiated in only 8 out of 24 specimens. After splitting the specimens and removing the rebar (WE), corrosion was clearly visible in those cases where the electrochemical measurements had indicated depassivation, and no signs of corrosion were found when checked in the other samples. In case of corrosion, red rust was found on both the steel and the concrete at the steel/concrete interface (Fig. 9). In general, one or a few pits were observed within a small area (a few mm²), while the rest of the rebar did not show any signs of corrosion. Sometimes, the corrosion products had spread out up to 1 cm away from the pit. With one exception (PC-05-2), pitting always exclusively initiated on the back side of the rebar (with respect to the direction of chloride ingress). In sample PC-05-2, some tiny pits were also found on the front side of the rebar; however, since the corrosion spot was larger on the back side, it can reasonably be assumed that pitting first started on the back side as in the other depassivated samples.

Regarding the concrete at the interface, macropores (air voids) were usually present with diameters up to several millimetres

(Fig. 9). The location of corrosion onset did, however, never coincide with the location of macropores. Another striking observation made in all split samples, regardless of whether corrosion started or not, is that the concrete in contact with the front side of the rebar was whitish; the other side of the rebar had a darker grey colour (Fig. 9). Remember that during casting, the specimens were placed up-side-down (casting direction identical with direction of chloride ingress, Fig. 1), and thus the side exhibiting the white surface was on top of the rebar during casting. In addition, it was in many cases observed that concrete adhered well to the steel surface on the side that was up during casting, whereas on the lower side, no concrete stuck to the rebar.

3.5. Chloride profiles

Chloride ion activities in the pore solution at depth $d = 10$ mm were continuously measured with the embedded ISEs; acid-soluble chloride contents, here assumed as total chloride contents, were measured at various depths in the end (t_{split}). Fig. 10 shows chloride profiles of different mixes obtained after exposure times ≥ 388 d (with the exception of PC-06-1 that was split at $t = 300$ d). Mean values were plotted from all measured profiles within a mix, with the exception of series SR-05 and SRFA-05, where samples that have been identified to behave differently were plotted separately (compare monitoring of resistivity and free chlorides). All profiles apart from PC-04 and PC-06 have a maximum at 3–4 mm. The chloride contents are lower in mix PC-04 than in PC-05 (at comparable ages), and clearly higher in PC-06 even at a younger age (ca. 5 months earlier); no significant differences are observed between PC-05 and SR-05. It is interesting to compare fly ash containing mixes with those produced from pure Portland or SR cement ($w/b = 0.5$): In the outermost millimetres (0–10 mm), the total chloride content is higher in FA containing mixes, but at depths > 10 mm, the chloride content is lower (Fig. 10b). The chloride profile is thus steeper in the case of FA.

In this paper, the measured chloride concentrations are termed as follows:

- $a_{Cl,10}^{stable}$, chloride ion activity in the pore solution (mol/l) at t_{stable} at $d = 10$ mm.
- $a_{Cl,10}^{split}$, chloride ion activity in the pore solution (mol/l) at t_{split} at $d = 10$ mm.
- $c_{L,x}^{split}$, total chloride content (% by binder weight) at t_{split} at depth $d = x$ (in mm).
- $c_{t,p}^{split}$, total chloride content (% by binder weight) at t_{split} at $d = p$, where p is the depth at which corrosion was visually detected (compare Table 5).

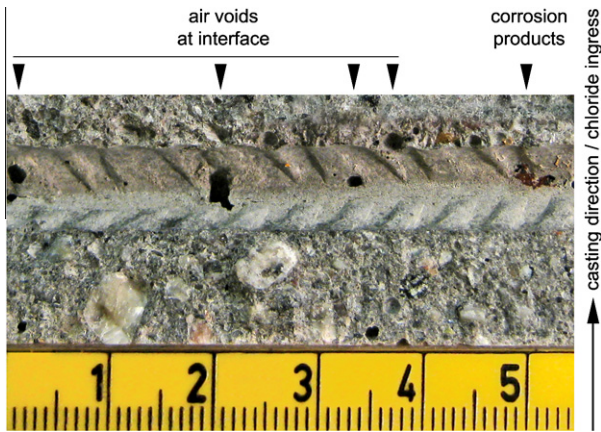


Fig. 9. Example of steel/concrete interface after splitting and removing WE (specimen PC-05-2) showing entrapped air voids and corrosion products (red rust). Unit of ruler = cm. (For interpretation of the references to colour in this figure legend, the reader is referred to the web version of this article.)

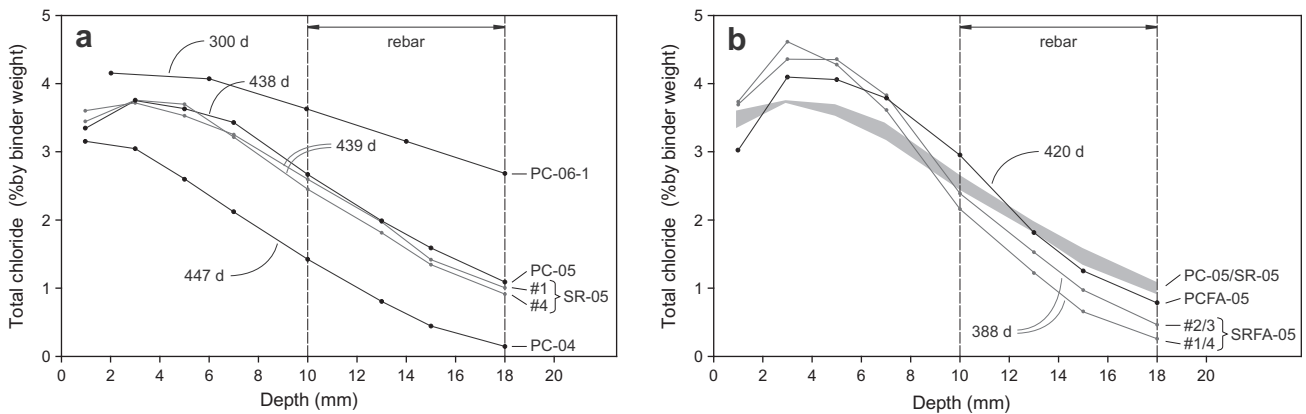


Fig. 10. Average chloride profiles for different mixes (t_{split} indicated for each curve).

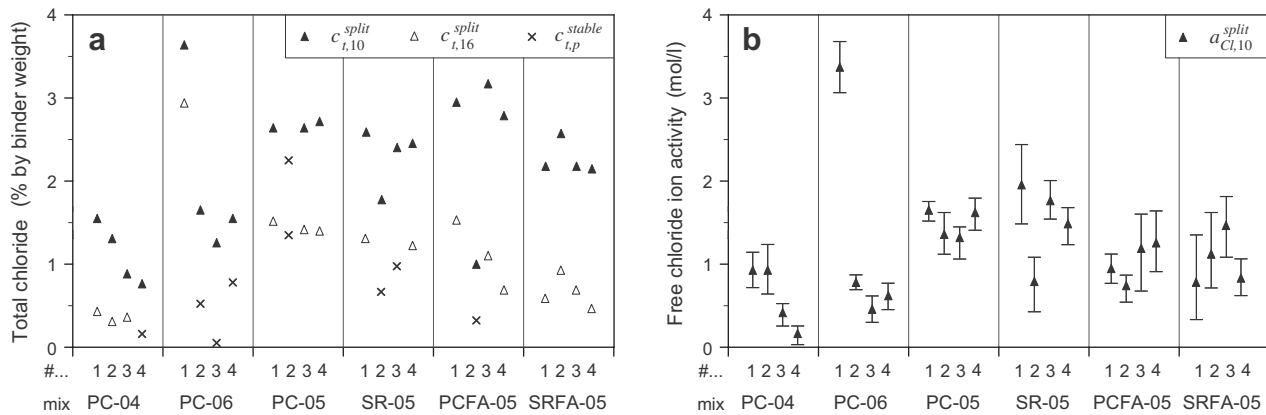


Fig. 11. Total (a) and free (b) chlorides measured at t_{split} (triangles) as well as estimated at t_{stable} (\times). Black symbols indicate depth 10 mm (front side); empty symbols represent depth 16 mm (back side). The four data points per mix are the four parallel specimens from #1 to #4. The whiskers in (b) represent the 10% and 90% percentiles and the triangle the average of the six ISEs per specimen.

The acid-soluble chloride contents were measured after corrosion initiation and thus slightly overestimate the critical chloride content. Since the free chloride ion activity in the pore solution is known at all times, back calculation is possible and total chloride contents at t_{stable} can be estimated. This has been done as explained in detail in Appendix A. Of particular interest is the following variable:

$c_{t,p}^{stable}$, total chloride content (% by binder weight) at t_{stable} at depth $d = p$.

Fig. 11 shows total and free chlorides at relevant depths and points in time. Front and back sides of the rebar were considered separately. Symbol \times stands for the chloride content associated with corrosion onset, i.e. it can be regarded as the critical chloride content (at depth p). In many cases, however, corrosion did not start and thus the measured chloride contents indicate that the chloride threshold is at least as high (triangles pointing upwards in Fig. 11).

4. Discussion

4.1. Depassivation detection by electrochemical measurements

In the passive state, the potentials of both WE and UR ranged from -200 to -70 mV vs. SCE before and after starting exposure to chloride (Table 4, Figs. 2 and 3), which is in agreement with values observed in field structures exposed to the atmosphere [12,13]. The observed continuous asymptotic potential increase is most likely owing to passive layer growth (thickening and transformation regarding composition and oxidation state) and the associated reduction in passive current density [14–16]. In the presence of fly ash, an additional possible reason contributing to the raise in potential is the decrease in pH over time that occurs owing to the pozzolanic reaction [4,17,18].

Figs. 2 and 4 show that the shape of potential vs. time curves during transition from clearly passive to clearly active condition can be very different. It is evident that detection of depassivation is not always straightforward. In this work, two distinct points in time, t_{ini} and t_{stable} , have been identified and three different cases were distinguished with examples shown in Fig. 4: (a) sudden drop in potential, (b) slow potential decrease, and (c) depassivation/repassivation. Whereas in case (a) stable conditions for corrosion propagation are achieved fast (within 1 or 2 d), significantly more time is required in case (b). A corrosion spot is obviously formed

(t_{ini}) that is only capable of polarising the rebar slightly into the negative direction and depress the overall R_p of WE to an extent outside the measurement resolution of the used datalogger. Only after more time has passed (and further exposure to wetting/drying cycles and thus chloride ingress has taken place), the active area becomes able to polarise the complete rebar by several hundreds of millivolts (t_{stable}). Case (c) describes specimens that repassivated after a pronounced potential decrease and then remained passive for up to 1 year of further chloride exposure. Apparently, the chloride concentration at t_{ini} can be sufficiently high to initiate pitting, but might not necessarily be able to sustain stable pit growth.

Thus, under the present conditions (non-polarised steel, cyclic wetting/drying), transition from clearly passive to clearly active takes place in many cases over a long period of time, and also over a range of chloride concentrations rather than a single value. As an example, the chloride ion activity at the embedded ISEs in sample SR-05-2 rose from 0.25 mol/l at t_{ini} to 0.55 mol/l at t_{stable} ; in sample PC-05-2 from 1.1 mol/l to 1.4 mol/l. Also other authors have pointed out that depassivation must be considered as a period of time during which the process from initial pit formation until stable corrosion takes place, rather than an instant event [19]. Although t_{ini} is closer to depassivation (i.e. nucleation of one or several pits) than t_{stable} , it is from an engineering viewpoint not relevant for describing corrosion-onset and measuring the critical chloride content. Regarding practice, corrosion-onset might be defined by the time at which stable pit growth is possible, i.e. t_{stable} .

4.2. Role of steel/concrete interface

In this work, corrosion never initiated at the location of air voids entrapped at the steel/concrete interface. This is not surprising when considering that owing to the exposure conditions, air voids never become saturated. The same was found earlier by the present authors and discussed in more detail in Ref. [20].

The fact that corrosion almost exclusively started on the back side of the rebar – and thus on the side with a lower chloride concentration – was ascribed to the effect of casting direction [20]: The steel/concrete interfaces formed on the upper and lower sides of the rebar during casting exhibit different characteristics. Effects such as collection of bleeding water and plastic settlement (formation of a gap) [21,22] or local higher w/b ratio and porosity [23,24] might weaken the interface on the lower half of the rebar and present more likely initiation sites than on the opposite side. In this work, the upper side of the steel (good interface) was closer to the sample surface in contact with chloride solution (depth

10–14 mm) than the lower side (bad interface, depth 14–18 mm) (Fig. 1). Differences in concrete characteristics between these two sides were visually confirmed by the presence of the observed whitish surface on the front side of the interfacial concrete after removing the steel and the fact that concrete adhered well to the steel on the front side but not on the back side (compare Section 3.4). Further experiments are currently carried out to study the effect of casting direction and the steel/concrete interface in more detail.

4.3. Determination of the chloride content

In this work, two independent methods have been applied to determine the chloride content in concrete: ion selective electrodes determined the *free chloride concentration* in the pore solution at 10 mm depth (Figs. 7 and 8) and the *total (acid soluble) chloride content* was determined by profile cutting/grinding (Fig. 10).

Ion selective electrodes respond to ions in direct vicinity of their surfaces (ions that interact with the membrane) and give thus highly localised results. Possible error sources are geometrical positioning (not exactly at the same depth) and the presence of diffusion potentials between ISE and reference electrode [25–27]. In this work, both these effects can however be considered negligible. If, for instance, the true junction potential deviated from the assumed values (see Section 2.2) by 2–5 mV, which is considered a realistic error, the corresponding error in chloride ion activity would be 10–20%. Regarding internal membrane potentials, it has been shown that these are negligibly small as long as the pH is high [25,26]. While this is the case in PC-mixes, the measurements in fly ash containing concrete might be associated with a somewhat larger uncertainty.

Figs. 7 and 8 reveal that the chloride ion activity in the concrete pore solution varies considerably at the constant depth of 10 mm (at a certain time). Even when evaluating concrete specimens separately, the six embedded ISEs scatter by ca. 0.2–1.0 mol/l (apparent from the individual curves in Fig. 7 and from 10%- to 90%-percentiles in Fig. 8b). Considering that concrete is an inhomogeneous material, both on a microscopic as well as on a macroscopic level, it is not surprising that chloride ingress occurs in a non-uniform manner and that thus, the chloride concentration is not constant at a certain depth. This was also observed by other researchers [28].

In contrast to the highly localised information provided by ISEs, procedures for analysis of acid-soluble chlorides in concrete require a certain minimum amount of concrete powder, typically 3–10 g [29,30], and thus result in an average value over the studied sample volume (ca. 1–5 cm³). Possible error sources are the ratio between aggregate and cement paste, which, particularly in small samples, might not be representative for the bulk concrete. Chloride contents obtained from concrete powder analysis have thus a limited spatial resolution. As shown in this work, corrosion does not necessarily initiate at the highest local chloride concentration. The reason for this is that other factors such as the conditions at the interface also determine the location of depassivation. Thus, the chloride content obtained from concrete powder may either over- or under-estimate the local critical chloride content.

4.4. Assessing cement types and concrete mixes regarding corrosion risk

When studying different concrete mixes in the laboratory in order to assess the risk for corrosion, two mechanisms can be considered separately for the initiation stage: (1) the resistance of the concrete against penetration of aggressive species, and (2) the chloride concentration at the steel surface required to initiate

corrosion. The first point describes mass transport through the concrete, and the second the critical chloride content, which is a matter of electrochemistry as well as physical and chemical characteristics of the steel/concrete interfacial zone.

4.4.1. Concrete resistivity and resistance against chloride penetration

Since the exposure conditions for the different mixes were similar, the data plotted in Fig. 8 is a measure for the chloride penetration resistance of the cover concrete. As expected, the chloride ion activity in the pore solution at 10 mm depth rises significantly faster at higher w/b ratios. The chloride concentration at for instance $t = 300$ d (Fig. 8b) increases in the order $w/b = 0.4 < 0.5 < 0.6$, where the difference from $w/b = 0.5$ to 0.6 is clearly higher (95% confident lower bound for difference at $t = 300$ d, here denoted $\Delta_{0.95} = 1.93$ mol/l) than from 0.4 to 0.5 ($\Delta_{0.95} = 0.29$ mol/l). This is also reflected by the slope of the curves in Fig. 8a. Regarding the effect of binder, SR cement shows a slightly higher increase in free chloride concentration than PC cement ($\Delta_{0.95} = 0.07$ mol/l), which might be explained by the lower chloride binding capacity of SR cement [31]. In combination with 20% fly ash, the increase of free chloride concentration vs. time is decelerated for both Portland and SR cement. At a younger age ($t = 60$ d), the relative performances of the mixes are somewhat different. For instance, PCFA-05 performs clearly worse than PC-05. Samples PC-06, on the other hand, show a significantly higher chloride content than the other mixes also at this age.

It is well recognised that there exists a relation between resistivity and chloride diffusion, viz. an increase in diffusion coefficient with lower resistivity, e.g. Refs. [32,33]. Both resistivity and diffusion coefficient are measures of ionic flow through concrete microstructure. Moreover, it was also observed that the corrosion rate is inversely proportional to concrete resistivity [34–38]. Thus, resistivity can be considered as a general parameter for describing performance of reinforced concrete structures subject to chloride exposure, both regarding the initiation and the propagation stage. The increase of resistivity with decreasing w/b ratio, apparent from Fig. 6, has also been reported by other authors [32,36,39,40]. As already indicated by the data regarding chloride penetration (Fig. 8), the difference between $w/b = 0.6$ and 0.5 is larger than between 0.5 and 0.4 . This might be explained by the fact that $w/b = 0.6$ appears to be beyond the disputed borderline between pastes that can and pastes that cannot achieve discontinuous capillary porosity [41,42]. The relation between resistivity and chloride ingress, plotted in Fig. 12, shows that the higher the concrete resistivity of the cover zone, the lower is the amount of chloride that reaches a certain depth (here 10 mm) after a given time. This is clearly apparent for the Portland cement mixes with $w/b = 0.4, 0.5$ and 0.6 . For the fly ash containing mixes PFCA and SRFA, comparatively high chloride concentrations are present despite high resistivities, particularly at a young age (Fig. 12a). This can be explained by the slow cement hydration process [18], allowing chloride ions to penetrate easily during the first wetting/drying cycles when most of the fly ash had not yet reacted. At a later age (Fig. 12b), the differences between mixes with and mixes without fly ash are lower. Taken as durability parameter, the present results for resistivity (Fig. 6) are generally in agreement with the monitored chloride ingress (Figs. 7 and 8): For mixes with high resistivity, comparatively longer times are required to reach a certain chloride ion activity at depth 10 mm.

As apparent from Fig. 6, the resistivity continues increasing with time, most markedly in the presence of fly ash or at $w/b = 0.4$, but slightly also in the mixes with $w/b = 0.5$ and 0.6 . This might be explained by the progressing refinement of the pore structure due to continuing cement hydration, and in addition, in the case of fly ash, the slow pozzolanic reaction [18]. Values up to three times as high were measured in fly ash containing mixes

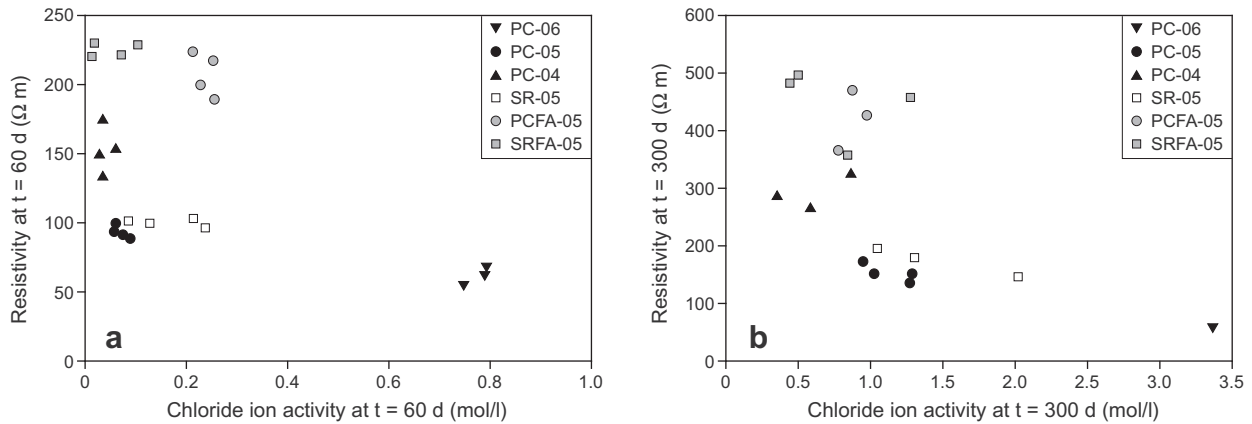


Fig. 12. Resistivity vs. chloride ion activity in the pore solution; (a) at $t = 60$ d and (b) at $t = 300$ d. Plotted for individual concrete specimens, i.e. resistivity as average from 2 measurements and chloride ion activity as average from 6 ISEs.

compared with the case of ordinary Portland cement (600 Ω m vs. 200 Ω m after ca. 1 year (Fig. 6). The beneficial effect of fly ash, viz. the potential to significantly raise the resistivity on the long-term, has also been observed by other researchers [32,33,36]. However, Figs. 6 and 8 have in addition shown that FA-mixes are particularly vulnerable at young ages. Note that also in terms of compressive strength measured at 28 d (Table 3), FA containing mixes perform worse than the corresponding mixes without FA. Thus, any experimental observations made at young ages are not suitable to predict the long-term behaviour of mixes containing fly ash.

The beneficial effect of a low w/b ratio on the rate of chloride ingress is confirmed by the chloride profiles of the total chloride content (Fig. 10). The observation that steeper profiles are obtained for fly ash containing mixes is in agreement with results by Polder [43] from similar experiments. This effect has been explained by the higher chloride binding capacity of FA concrete [44]. Regarding durability, this is favourable since it decreases the chloride content at depths where the reinforcement is usually located in practice. In this study, however, the total chloride content at depth 10 mm, where the front side of WE is situated, is similar for mixes with and without FA (w/b = 0.5). At depth 18 mm (back side of WE), on the other hand, the FA mixes have lower chloride contents than the other mixes.

4.4.2. Critical chloride content

Also the chloride concentration associated with corrosion onset (t_{stable}) is an indicator for assessing the corrosion risk. Despite rather high chloride contents, in this study stable corrosion established only in one third of the samples. In case it did, this occurred preferably on the back side of the rebar, although the chloride content on the front side was considerably higher (Fig. 10). Fig. 11a shows the total chloride content at depth 10 mm (black-filled triangles) and depth 16 mm (open triangles) for all samples. The black-filled triangles in Fig. 11a can be considered as minimum values for the critical chloride content on the front side of the rebar since at these contents corrosion did not initiate. The values scatter considerably owing to the often large differences in t_{split} between parallel samples (Table 5), but lie generally on high levels ranging from 0.8% to 3.6% chloride by binder mass. For comparison, threshold values above 3% chloride by binder mass are seldom reported in the literature [3]. Regarding the back side of the rebar, corrosion onset is associated with rather low total chloride contents in some cases, whereas the steel remains in passive condition at clearly higher values in other samples of the same mix (PC-04, PC-06, and PCFA-05 in Fig. 11a). These values are however likely to be misleading since they are based on measurements on powdered

concrete taken from the concerning depth. As discussed above, the local chloride concentration at the steel/concrete interface might differ considerably from this average value (also because the interfacial transition zone around the rebar is likely to offer a faster penetration path for chlorides to reach the back side of the steel than in bulk concrete). Nevertheless, it is apparent that the critical chloride content is different for both rebar sides.

High chloride threshold values obtained in laboratory setups are usually associated with unrealistically good conditions during casting (labcrete) compared with practice (realcrete). In this study, however, large air voids were visually observed on both sides of the steel/concrete interface (Fig. 9). The high level of threshold values can thus not be ascribed to defect-free labcrete. Another possible explanation for unrealistically high critical chloride contents is the effect of specimen size, viz. an increasing susceptibility to pitting corrosion with increasing exposed steel area. This effect was observed in experiments dealing with steel immersed in aqueous solutions [45–47] and the concept was recently developed further for reinforcement embedded in concrete [48]. From these results, also the scatter is expected to rise with decreasing specimen size. In this study, both high levels as well as a high scatter of critical chloride contents were found. This has also been the case in other investigations with similar sample sizes, as summarised in Ref. [3]. The fact that a concrete specimen with w/c = 0.6 (PC-06-1) remains passive even at a high (average) chloride content in the range 3.0–3.6% chloride by cement weight, supports the hypothesis that coincidence of a local interfacial or metallurgical defect and a sufficiently high local chloride concentration is required for depassivation. It is evident that the probability for such a coincidence rises with increasing area of exposed steel. Theoretically, also other reasons might have been responsible for the distinct behaviour of sample PC-06-1. However, none of the performed measurements or experimental observations (e.g. cover concrete quality (air voids), passive steel potential) indicated that this specimen differed from the others of series PC-06. It was also subjected to exactly the same experimental treatment as the other specimens.

4.4.3. Qualitative assessment of concrete mixes

When evaluating the concrete mixes with respect to their susceptibility to corrosion, particularly the effects of binder and w/b ratio might be of interest. On a theoretical basis, fly ash is expected to improve the quality of the steel/concrete interface due to its effects on the concrete microstructure [18] and is thus thought to increase the chloride threshold value. Moreover, fly ash improves the chloride binding of the cement paste [31,49,50], but

Table 6
Ranking of the studied concrete mixes regarding corrosion risk.

Ranking criterion	Best performance – worst performance
Resistivity (for $t > 90$ d)	PCFA-05/SRFA-05 > PC-04 > PC-05/SR-05 >> PC-06
Free chloride ion activity vs. time ($t \approx 60$ d)	PC-04/PC-05/SRFA-05 > SR-05/PCFA-05 >> PC-06
Free chloride ion activity vs. time ($t \approx 300$ d)	PC-04/PCFA-05/SRFA-05 > PC-05/SR-05 >> PC-06
Time to corrosion (t_{stable})	SRFA-05 > PC-05 > PC-04/PCFA-05 > SR-05 > PC-06

on the other hand, it is known to reduce the pH of the pore solution [4,17,18] and might thus render embedded steel more susceptible to corrosion. In the literature, contradictory chloride threshold values have been reported for fly ash: While the authors of Refs. [51–53] found lower critical chloride contents for fly ash containing cements, an improved corrosion resistance was reported in Refs. [54,55]. Regarding sulphate resistant cement, its lower chloride binding capacity [31] is expected to result in lower chloride threshold values when expressed in terms of total chlorides. This was experimentally confirmed in Refs. [6,52]; Alonso et al. [56], on the other hand, did not find significant differences between pure Portland cement, SR cement and fly ash containing cement. In contrast to the influence of binder, the effect of w/b ratio, viz. increasing threshold values for lower w/b ratios, is well documented in the literature, e.g. Ref. [57].

The parameters shown in Figs. 6 and 8 as well as the times to corrosion given in Table 5 provide a basis for a ranking of the studied concrete mixes with regard to corrosion risk. The relative performances are shown in Table 6. Also in this study, PC-06 performs worse than the other mixes since only in this series, 3 out of 4 samples depassivated. Regarding the effect of fly ash, only 1 of the 8 fly ash containing samples started corrosion. However, the chloride content on the back side of WE was lower in these samples compared with PC or SR cement samples made with the same w/b ratio owing to the steeper chloride profiles (Fig. 10). In addition, the scatter of the results (e.g. Fig. 11) is so high that comparison between the mixes can only be made with a low level of confidence. To improve the data, a higher amount of parallel samples would be required.

In summary, low w/b ratios and fly ash are clearly beneficial on a long-term basis. Nevertheless, the binder type seems to be a less dominant factor than the conditions at the steel/concrete interface (casting direction).

5. Conclusions

From this study, the following major conclusions can be drawn:

- (1) Transition from the passive to a clearly active state can under open circuit conditions occur over a long period of time rather than a well-defined instant. In addition, it was observed in many cases that after the first signs of depassivation, a marked increase in chloride content was required to prevent repassivation and to enable stable pit growth. If in a laboratory setup, the chloride content is measured at the very first depassivation event, it might thus be too conservative for engineering purposes in practice.
- (2) Cement replacement with fly ash has beneficial effects regarding chloride penetration resistance as well as electrical resistivity of the concrete. The same improvements are seen when decreasing the w/b ratio. However, fly ash containing mixes are particularly vulnerable to chloride exposure at young ages.

- (3) With respect to corrosion performance, by far the most dominant influencing parameter was found to be the steel/concrete interface since corrosion almost always exclusively initiated on the back side of the rebar (with respect to casting direction and chloride ingress) regardless of binder type and w/b ratio. On this side, the interface is expected to be worse owing to plastic settlement and collection of bleeding water. Considering the direction of chloride ingress, however, the chloride content is higher on the front side of the rebar. Thus, corrosion does not necessarily initiate where the highest chloride content occurs.
- (4) The free chloride ion activity in the pore solution varies considerably even at a constant depth. Since common sampling and analysis techniques such as for acid-soluble chloride content provide average values over a certain concrete volume, the critical chloride content might be over- or underestimated. Knowledge of the spatial variability of total chloride contents is required in order to be able to treat this uncertainty statistically.
- (5) In many specimens, no corrosion started even at significantly higher chloride concentrations than in the corroding parallel samples. Considering that the local chloride concentration as well as interfacial or metallurgical defects exhibit spatial variability, this implies that only coincidence of the latter with a sufficiently high local chloride concentration leads to depassivation.

Acknowledgement

The work described in this paper forms part of the Norwegian COIN project (<http://coinweb.no>).

Appendix A

The measured profile of acid-soluble (total) chlorides at time t_{split} was empirically fitted to the following equation:

$$c_{t,x}^{split} = c(x, t_{split}) = u \cdot \operatorname{erfc}\left(\frac{x}{v\sqrt{t_{split}}}\right) \quad (\text{A.1})$$

Here, $c(x, t_{split})$ is the chloride content in mass percent by binder at depth x (mm) and u and v are fitting parameters. Good solutions were obtained when u was set equal to the y-intercept of the extrapolated linear branch of the chloride profile (at $x = 0$). The chloride content associated with corrosion onset is here considered as the chloride content at t_{stable} and depth p according to Table 5, i.e. $c_{t,p}^{stable}$, and can then be estimated with Eq. (A.1) by replacing t_{split} with t_{stable} and for $x = p$. To check if the estimate is reasonable, $c_{t,10}^{stable}$ was also calculated and compared to the value obtained from the following reasoning: Changes in free chloride ion activity from t_{stable} to t_{split} are known (at 10 mm depth). Under the assumption that these are reflected in total chloride contents and follow a certain chloride binding relationship, $c_{t,10}^{stable}$ can be estimated. From evaluation of measured free ($a_{cl,10}^{split}$) vs. total ($c_{t,10}^{split}$) chloride contents, it was found that chloride binding can reasonably be approximated by a linear fit with slope m (at least in the range of the relevant concentrations). Thus,

$$c_{t,10}^{stable} = c_{t,10}^{split} - \frac{a_{cl,10}^{split} - a_{cl,10}^{stable}}{m} \quad (\text{A.2})$$

The values for $c_{t,10}^{stable}$ obtained from the described two procedures were in good agreement (difference <20%) for all cases except for PC-06-3, that showed a bad error function fit owing to the steep chloride profile at the relatively short exposure time ($t_{stable} = 13$ d).

It is recognised that these estimations might be uncertain. Nevertheless, considering the large scatter in local chloride content (indicated by the individual values of the embedded ISEs), any inaccuracies associated with the error function approach (Eq. (A.1)) are of minor significance. As the time differences between t_{stable} and t_{split} are in most cases small (with respect to total exposure time), the estimated profile at t_{stable} is not too different from the measured (and fitted) one at t_{split} .

References

- [1] K. Tuutti, Corrosion of steel in concrete, Swedish Cement and Concrete Research Institute, 1982.
- [2] G.K. Glass, N.R. Buenfeld, Chloride threshold levels for corrosion induced deterioration of steel in concrete, in: L.O. Nilsson, J.P. Ollivier (Eds.), Proc. RILEM Int. Workshop "Chloride penetration into concrete", Paris, 1997, pp. 429.
- [3] U. Angst, B. Elsener, C.K. Larsen, Ø. Vennesland, Critical chloride content in reinforced concrete – A review, *Cem. Concr. Res.* 39 (2009) 1122–1138.
- [4] K. Byfors, Influence of silica fume and flyash on chloride diffusion and pH values in cement paste, *Cem. Concr. Res.* 17 (1987) 115–130.
- [5] P. Lambert, Corrosion and passivation of steel in concrete, PhD Thesis, Aston University, 1983.
- [6] P. Lambert, C.L. Page, P.R.W. Vassie, Investigations of reinforcement corrosion. 2. Electrochemical monitoring of steel in chloride-contaminated concrete, *Mater. Struct.* 24 (1991) 351–358.
- [7] B. Elsener, L. Zimmermann, H. Böhm, Non destructive determination of the free chloride content in cement based materials, *Mater. Corros.* 54 (2003) 440–446.
- [8] U. Angst, B. Elsener, C.K. Larsen, Ø. Vennesland, Potentiometric determination of the chloride ion activity in cement based materials, *J. Appl. Electrochem.* 40 (2010) 561–573.
- [9] W.J. McCarter, G. Starrs, T.M. Chrisp, Electrical monitoring methods in cement science, in: J. Benst, P. Barnes (Eds.), *Structure and Performance of Cements*, second ed., Spon Press, Taylor & Francis, London, 2002, pp. 442–456.
- [10] B.B. Hope, J.A. Page, A.K.C. Ip, Corrosion rates of steel in concrete, *Cem. Concr. Res.* 16 (1986) 771–781.
- [11] COMSOL Multiphysics V3.5a.
- [12] L. Bertolini, B. Elsener, P. Pedferri, R. Polder, Corrosion of steel in concrete, WILEY VCH, Weinheim, 2004.
- [13] B. Elsener, C. Andrade, J. Gulikers, R. Polder, M. Raupach, Half-cell potential measurements – potential mapping on reinforced concrete structures (RILEM TC 154-EMC recommendation), *Mater. Struct.* 36 (2003) 461–471.
- [14] D. Addari, B. Elsener, A. Rossi, Electrochemistry and surface chemistry of stainless steels in alkaline media simulating concrete pore solutions, *Electrochim. Acta* 53 (2008) 8078–8086.
- [15] S. Joiret, M. Keddah, X.R. Nóvoa, M.C. Pérez, C. Rangel, H. Takenouti, Use of EIS, ring-disk electrode, EQCM and Raman spectroscopy to study the film of oxides formed on iron in 1 M NaOH, *Cem. Concr. Comp.* 24 (2002) 7–15.
- [16] A. Rossi, G. Puddu, B. Elsener, The surface of iron and Fe10Cr alloys in alkaline media, in: M. Raupach, B. Elsener, R. Polder, J. Mietz (Eds.), *Corrosion of reinforcement in concrete*, EFC Publication No. 38, Woodhead Publishing, Cambridge, 2007, pp. 44–61.
- [17] S. Diamond, Effects of two danish flyashes on alkali contents of pore solutions of cement-flyash pastes, *Cem. Concr. Res.* 11 (1981) 383–394.
- [18] K. Luke, Pulverized fuel ash as a cement extender, in: J. Benst, P. Barnes (Eds.), *Structure and Performance of Cements*, second ed., Spon Press, Taylor & Francis, London, 2002, pp. 353–371.
- [19] COST 521: Final report "Corrosion of steel in reinforced concrete structures", Luxembourg, 2002.
- [20] U. Angst, C.K. Larsen, Ø. Vennesland, B. Elsener, Influence of casting direction on chloride-induced rebar corrosion, in: P. Castro-Borges, E.I. Moreno, K. Sakai, O. Gjörv, N. Banthia (Eds.), *CONSEC'10 6th Int. Conf. on Concrete under Severe Conditions, Environment and Loading*, vol. 1, Taylor & Francis, London, 2010, pp. 359–366.
- [21] T.A. Soylev, R. Francois, Corrosion of reinforcement in relation to presence of defects at the interface between steel and concrete, *J. Mater. Civ. Eng.* 17 (2005) 447–455.
- [22] T.A. Soylev, R. Francois, Quality of steel-concrete interface and corrosion of reinforcing steel, *Cem. Concr. Res.* 33 (2003) 1407–1415.
- [23] C.L. Page, Initiation of chloride-induced corrosion of steel in concrete: role of the interfacial zone, *Mater. Corros.* 60 (2009) 586–592.
- [24] A.T. Horne, I.G. Richardson, R.M.D. Brydson, Quantitative analysis of the microstructure of interfaces in steel reinforced concrete, *Cem. Concr. Res.* 37 (2007) 1613–1623.
- [25] U. Angst, Ø. Vennesland, Detecting critical chloride content in concrete using embedded ion selective electrodes – effect of liquid junction and membrane potentials, *Mater. Corros.* 60 (2009) 638–643.
- [26] U. Angst, B. Elsener, R. Myrdal, Ø. Vennesland, Diffusion potentials in porous mortar in a moisture state below saturation, *Electrochim. Acta* 55 (2010) 8545–8555.
- [27] U. Angst, Ø. Vennesland, R. Myrdal, Diffusion potentials as source of error in electrochemical measurements in concrete, *Mater. Struct.* 42 (2009) 365–375.
- [28] N. Silva, L. Tang, S. Rauch, An innovative approach for measuring chloride threshold levels in reinforced concrete, in: R.M. Ferreira, J. Gulikers, C. Andrade (Eds.), 3rd Int. PhD Workshop on Modelling the Durability of reinforced Concrete, RILEM, Guimarães, Portugal, 2009, pp. 28–34.
- [29] SIA 162/2, Quantitative Bestimmung des Chloridgehalts von Beton (2001), Schweizer Ingenieur- und Architektenverein. (in German).
- [30] ASTM C-1152, Standard test method for acid-soluble chloride in mortar and concrete, American Society for Testing and Materials.
- [31] C. Arya, N.R. Buenfeld, J.B. Newman, Factors influencing chloride-binding in concrete, *Cem. Concr. Res.* 20 (1990) 291–300.
- [32] R.B. Polder, W.H.A. Peelen, Characterisation of chloride transport and reinforcement corrosion in concrete under cyclic wetting and drying by electrical resistivity, *Cem. Concr. Compos.* 24 (2002) 427–435.
- [33] P.A.M. Basheer, P.R.V. Gilleece, A.E. Long, W.J. Mc Carter, Monitoring electrical resistance of concretes containing alternative cementitious materials to assess their resistance to chloride penetration, *Cem. Concr. Compos.* 24 (2002) 437–449.
- [34] A. Molina, C. Andrade, C. Alonso, J.A. González, Factores controlantes de la velocidad de corrosión de las armaduras embebidas en morteros de cemento (in spanish), *Rev. Téc. Ing., Univ. Zulia* 8 (1985) 9–15.
- [35] G.K. Glass, C.L. Page, N.R. Short, Factors affecting the corrosion rate of steel in carbonated mortars, *Corros. Sci.* 32 (1991) 1283–1294.
- [36] L. Bertolini, R.B. Polder, Concrete resistivity and reinforcement corrosion rate as a function of temperature and humidity of the environment, TNO report 97-BT-R0574, TNO Building and Construction Research, Delft, The Netherlands, 1997.
- [37] W. Morris, A. Vico, M. Vazquez, S.R. de Sanchez, Corrosion of reinforcing steel evaluated by means of concrete resistivity measurements, *Corros. Sci.* 44 (2002) 81–99.
- [38] W. Morris, A. Vico, M. Vázquez, Chloride induced corrosion of reinforcing steel evaluated by concrete resistivity measurements, *Electrochim. Acta* 49 (2004) 4447–4453.
- [39] G.E. Monfore, The electrical resistivity of concrete, *J. PCA Res. Dev. Lab.* 10 (1968) 35–48.
- [40] C.K. Larsen, J.-M. Østvik, E.J. Sellevold, Ø. Vennesland, Electrical resistivity of concrete, part III: long term field measurements on concrete elements in the tidal zone, in: J. Marchand, B. Bissonnette, R. Gagné, M. Jolin, F. Paradis (Eds.), 2nd Int. Symp. on Advances in Concrete through Science and Engineering, RILEM, Quebec City, Canada, 2006.
- [41] T.C. Powers, L.E. Copeland, H.M. Mann, Capillary continuity or discontinuity in cement pastes, *J. PCA Res. Dev. Lab.* 10 (1959) 38–48.
- [42] G. Ye, Percolation of capillary pores in hardening cement pastes, *Cem. Concr. Res.* 35 (2005) 167–176.
- [43] R. Polder, Simulated de-icing salt exposure of blended cement concrete – chloride penetration, in: C. Andrade, J. Kropp (Eds.), Proc. 2nd International RILEM Workshop Testing and Modelling the Chloride Ingress into Concrete, RILEM Publications, Paris, 2000, pp. 189–202.
- [44] L.O. Nilsson, E. Poulsen, P. Sandberg, H.E. Sørensen, O. Klinghoffer, Chloride penetration into concrete – state of the art, HETEK report Nr. 53, 1996.
- [45] G.T. Burstein, G.O. Ilevbare, The effect of specimen size on the measured pitting potential of stainless steel, *Corros. Sci.* 38 (1996) 2257–2265.
- [46] L. Li, A.A. Sagüés, Chloride corrosion threshold of reinforcing steel in alkaline solutions – Effect of specimen size, *Corrosion* 60 (2004) 195–202.
- [47] M. Bettendorf, *Korrosionsangriffe am Armierungsstahl* (in German), Diplomarbeit, ETH Zürich, 1997.
- [48] U. Angst, A. Ronnquist, B. Elsener, C.K. Larsen, Ø. Vennesland, Probabilistic considerations on the effect of specimen size on the critical chloride content in reinforced concrete, *Corros. Sci.* 53 (2011) 177–187.
- [49] M. Kawamura, O.A. Kayyali, M.N. Haque, Effects of flyash on pore solution composition in calcium and sodium chloride-bearing mortars, *Cem. Concr. Res.* 18 (1988) 763–773.
- [50] O.A. Kayyali, M.N. Haque, The Cl^-/OH^- ratio in chloride-contaminated concrete – a most important criterion, *Mag. Concr. Res.* 47 (1995) 235–242.
- [51] M. Thomas, Chloride threshold in marine concrete, *Cem. Concr. Res.* 26 (1996) 513–519.
- [52] B.H. Oh, S.Y. Jang, Y.S. Shin, Experimental investigation of the threshold chloride concentration for corrosion initiation in reinforced concrete structures, *Mag. Concr. Res.* 55 (2003) 117–124.
- [53] H.-W. Song, M.-S. Jung, C.-H. Lee, S.-H. Kim, K.Y. Ann, Influence of chemistry of chloride ions in cement matrix on corrosion of steel, *ACI Mater. J.* 107 (2010) 132–139.
- [54] P. Schiessl, W. Breit, Local repair measures at concrete structures damaged by reinforcement corrosion – aspects of durability, in: C.L. Page, P.B. Bamforth, J.W. Figg (Eds.), Proc. 4th Int. Symp. "Corrosion of Reinforcement in Concrete Construction", The Royal Society of Chemistry, Cambridge, 1996, pp. 525–534.
- [55] Y.S. Choi, J.G. Kim, K.M. Lee, Corrosion behavior of steel bar embedded in fly ash concrete, *Corros. Sci.* 48 (2006) 1733–1745.
- [56] C. Alonso, M. Castellote, C. Andrade, Chloride threshold dependence of pitting potential of reinforcements, *Electrochim. Acta* 47 (2002) 3469–3481.
- [57] K. Pettersson, Chloride threshold value and the corrosion rate in reinforced concrete, in: K. Tuutti (Ed.), Proc. of the Nordic Seminar, 1995, pp. 257–266.